

Hidden magnetism, nonlinear magnetodielectric coupling, and large multicaloric effect in multiferroic L -type $\text{Fe}_2(\text{MoO}_4)_3$

P. Athira¹, Ajay Tiwari¹, M.-J. Hsieh,³ J.-Y. Lin,^{3,4} Nidhi Puri,³ C.W. Wang⁵, C. H. Prashanth¹, C. Dhanasekhar,¹ C.L. Huang,⁶ H.D. Yang^{2,7,*}, Krishnamurthy Jyothinagaram¹,[†] and D. Chandrasekhar Kakarla¹[‡]

¹Department of Physics, School of Sciences, National Institute of Technology, Tadepalligudem 534101, Andhra Pradesh, India

²Department of Physics, National Sun Yat-sen University, Kaohsiung, 80424, Taiwan

³Institute of Physics, National Yang Ming Chiao Tung University, Hsinchu 30010, Taiwan

⁴Center for Emergent Functional Matter Science, National Yang Ming Chiao Tung University, Hsinchu 30010, Taiwan

⁵National Synchrotron Radiation Research Center, Hsinchu, 30076, Taiwan

⁶Department of Physics and Center for Quantum Frontiers of Research & Technology (QFort), National Cheng Kung University, 701 Tainan, Taiwan

⁷Center of Crystal Research, National Sun Yat-sen University, Kaohsiung, 80424, Taiwan



(Received 30 November 2023; revised 7 February 2024; accepted 22 April 2024; published 13 May 2024)

$\text{Fe}_2(\text{MoO}_4)_3$ is a well-established L -type ferrimagnetic (L -FIM) material with field-induced magnetic ordering ($T_{\text{N}2}$) and multiferroic properties below $T_{\text{N}1}$ (around 12 K). In this study, we investigate the magnetic properties of $\text{Fe}_2(\text{MoO}_4)_3$ through temperature- and field-dependent ac and dc magnetic susceptibility $\chi(T)$ measurements. Isothermal magnetization data reveal an additional metamagnetic transition ($H_{\text{C}2}$) beyond the existing boundary between L -FIM and multiferroic phases ($H_{\text{C}1}$). Frequency-dependent ac magnetic susceptibility data demonstrate reentrant-spin-glass-like behavior below $T_{\text{N}1}$, with a critical temperature ($T_{\text{g}0}$) of 6.2 K. Notably, a nonlinear magnetodielectric response and concurrent anomalies in $M(H)$ at the two metamagnetic transitions ($H_{\text{C}1}$ and $H_{\text{C}2}$) allude to a profoundly intertwined magnetoelectric (ME) nature. A finite nonlinear ME effect (α_{ME}) of about 0.56 ps/m is comparable to that of ME materials such as NdCrTiO_5 and MnGa_2O_4 . The temperature-dependent adiabatic temperature change (ΔT_m) due to the contribution of magnetic spin entropy exhibits a small value (approximately 0.8 K) with an oscillatory-like magnetocaloric effect. Remarkably, the adiabatic temperature change (ΔT_{ME}) owing to magnetoelectric coupling is quite large (5.2 K under a 7 T magnetic field) near $T_{\text{N}2}$. The tunability of $T_{\text{N}2}$ with temperature and magnetic field strength represents a unique multicaloric medium whose temperature and field parameters can be easily adjusted for potential cryogenic applications near liquid-helium temperatures.

DOI: 10.1103/PhysRevApplied.21.054025

I. INTRODUCTION

The thermal response of solid materials to the simultaneous or sequential application of multiple external fields under adiabatic conditions is called the multicaloric effect [1–3]. Research efforts to explore large caloric effects in single-phase ferroic systems such as $\text{Ni}_{50}\text{Mn}_{35}\text{In}_{15}$ [4] and $\text{Gd}_5\text{Ge}_2\text{Si}_2$ [5,6] are supported by parallel studies of multicaloric phenomena with more than one caloric effect: magnetocaloric effect (MCE), electrocaloric effect (ECE),

elastocaloric, and barocaloric effects in multiferroics for solid-state refrigeration technology [7–12]. In addition to the conventional MCE and ECE, the coupling between ferroic ordered phases, for example, spin-induced ferroelectric materials [13–18], displays magnetoelectric (ME) coupling providing a third degree of freedom for adjusting multiple order parameters via a single external stimulus and providing improved adiabatic temperature changes. However, the number of such substances with multiple caloric effects in addition to individual caloric effects is limited. Lisenkov *et al.* theoretically estimated large multicaloric effects associated with ECE and elastocaloric effects in the multiferroic PbTiO_3 system [19], and more recently, NdCrTiO_5 [20] and Y_2CoMnO_6 [21] have also

*Corresponding author: yang@mail.nsysu.edu.tw

†Corresponding author: krishnamurthy@nitandhra.ac.in

‡Corresponding author: chandu@mail.nsysu.edu.tw

been shown to be susceptible to multicaloric effects caused by ME coupling. On the other hand, magnetization reversal induces an oscillatory magnetocaloric process accompanied by heating and cooling effects, and their coexistence in a homogeneous magnetic system provides benefits for the temperature stabilization of bath reservoirs [22–25]. Research on new materials exhibiting interesting magnetic phenomena alongside a multicaloric response holds significant promise for future technologies.

Recently, magnetic molybdate oxides $(\text{RE/TM})_2(\text{MoO}_4)_3$ (where RE, rare earth; TM, transition metal) have attracted great research attention due to their thermal expansion and multiferroic properties [26,27]. Rare-earth-based molybdate oxides $\text{Tb}_2(\text{MoO}_4)_3$ and $\text{Gd}_2(\text{MoO}_4)_3$ are ferroelectric and ferroelastic materials without soft polar modes [22,23]. On the other hand, $\text{Fe}_2(\text{MoO}_4)_3$ exhibits interesting magnetic properties and ferroelastic structural phase transitions (orthorhombic to monoclinic) at high temperatures [24,28,29]. The unit cell of $\text{Fe}_2(\text{MoO}_4)_3$ contains four different Fe sites. In the magnetically ordered phase, Mössbauer spectroscopy reveals two sextuplets with a sextuplet area ratio of $\alpha:\beta \sim 3:1$, indicating that three Fe sites share a similar hyperfine field. The difference between the hyperfine fields as a function of temperature exhibits a finite moment close to T_{N} , indicating weak ferrimagnetism arising from the incomplete compensation of antiferromagnetically coupled sublattices [30]. The slight differences in exchange interactions lead to different rates of thermal evolution for the two sublattice magnetizations. Despite the well-established *L*-type ferrimagnetic (*L*-FIM) nature, the ground-state spin structure and the spin orientation are not accurately resolved, and two contrasting spin structures have been proposed. Mössbauer analysis indicates that the magnetic moments lie in the ac plane, making an angle of 37° – 58° or 122° – 143° with the *c* axis [30]. On the other hand, neutron diffraction analysis proposes a collinear magnetic moment parallel to the [010] direction with the magnetic space group of $P2_1/a$ [31]. Ajay T. *et al.* reported exotic magnetic ordering induced by an external magnetic field (*H*), along with associated multiferroic behavior at $T_{\text{N}2}$, below the magnetic ordering of *L*-FIM at $T_{\text{N}1}$ [27]. The $T_{\text{N}2}$ and associated magnetoelectric phase were highly tunable with *H*. These results suggest that $\text{Fe}_2(\text{MoO}_4)_3$ might harbor complex magnetism beyond the existing *L*-FIM order. In this study, we explore a hidden magnetic glassy phase along with the field-induced magnetic boundaries. Furthermore, a non-collinear magnetoelectric coupling along with multicaloric properties is established.

II. EXPERIMENTAL DETAILS

Polycrystalline $\text{Fe}_2(\text{MoO}_4)_3$ samples were prepared via a conventional solid-state reaction technique, as previously described [32], and the detailed procedure is provided in

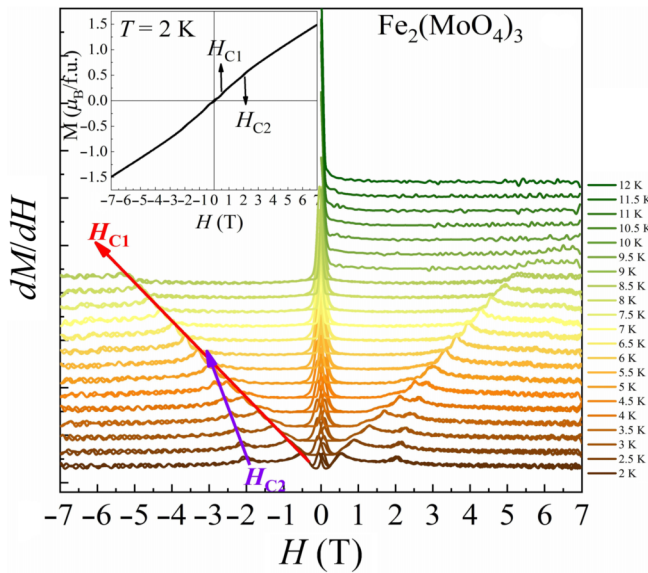
the Supplemental Material [33]. The sample purity was confirmed through in-house x-ray diffraction (XRD) analysis, which was conducted with a D8 Advance Bruker diffractometer using $\text{Cu } K\alpha_1$ radiation. The XRD data were analyzed using the FULLPROF_SUITE program [34], and the crystal structure was visualized using the VESTA software [35]. The details are provided in the Supplemental Material (Fig. S1) [33]. The surface morphology was investigated using field-emission scanning electron microscopy (FESEM; JEOL 6330F) along with energy-dispersive x-ray spectroscopy (EDS). In Fig. S2 in the Supplemental Material [33], an FESEM image is presented that illustrates randomly shaped grains with a size distribution ranging from 10 to 50 μm , separated by distinct grain boundaries. The quantitative areal analysis and elemental maps obtained via EDS reveal a uniform sample composition with a stoichiometric ratio Fe:Mo:O of 0.152:0.196:0.650. This ratio is consistent with the expected stoichiometry of $\text{Fe}_2(\text{MoO}_4)_3$, and the details are provided in the Supplemental Material (Table S2) [33]. The ac and dc magnetization measurements were performed utilizing a superconducting quantum interference device-based magnetometer (QD-MPMS-XL7). Specific heat capacity [$C_p(T, H)$] was measured using a heat-pulsed thermal relaxation calorimeter via a physical property measurement system setup. For transport measurements, we applied silver paste on both sides of a pellet sample with a thickness of approximately 0.8 mm to serve as electrodes. Temperature- and field-dependent dielectric [$\epsilon'(T, H)$] and polarization [$P(T, H)$] measurements were performed using an Agilent 4294A ($V_{\text{ac}} = 10$ V) *LCR* meter, and a Keithley 6517B electrometer, respectively. The $\epsilon'(T, H)$ and $P(T, H)$ measurements were performed with the sample geometry $H \perp E$.

III. RESULTS AND DISCUSSION

A. Hidden magnetism: Metamagnetic transitions and reentrant-spin-glass-like phase

Based on previously reported $\chi(T)$ data [27], it is imperative to elucidate the evolution of magnetization (*M*) in $\text{Fe}_2(\text{MoO}_4)_3$ with an external magnetic field (*H*). Initially, the $M(H)$ loop at 2 K [inset of Fig. 1(a)] manifests a predominantly linear variation of *M*, displaying no inclination towards saturation even under an $H = 7$ T field. The observed magnetization at 2 K amounts to $1.5 \mu_{\text{B}}/\text{f.u.}$, constituting approximately 15% of the total magnetization attributed to the spin-only contribution of Fe^{3+} magnetic spins. At lower *H*, the $M(H)$ loop exhibits finite hysteresis, suggesting a weak FIM nature [36]. However, upon meticulous examination of the $M(H)$ data at 2 K, specifically dM/dH vs *H*, two pronounced jumps at two metamagnetic transitions $H_{\text{C}1} = 0.5$ T and $H_{\text{C}2} = 2$ T become evident, as depicted in Fig. 1(a). To gain deeper insights into the evolution of $H_{\text{C}1}$ and $H_{\text{C}2}$, dM/dH vs

(a)



(b)

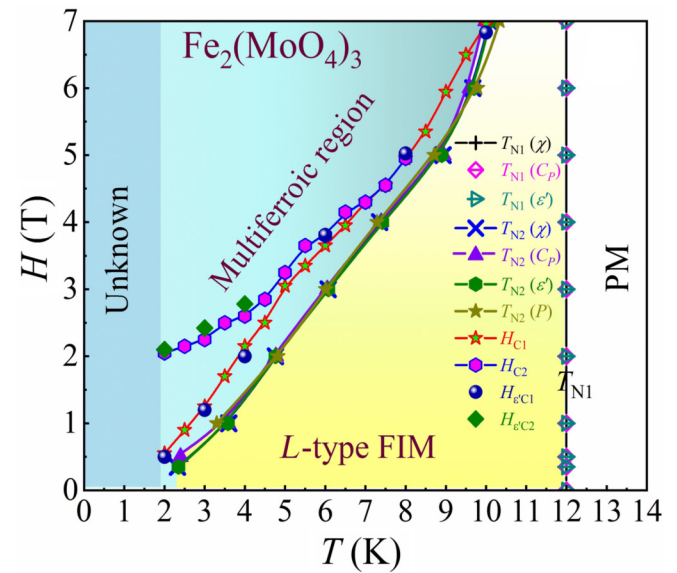


FIG. 1. (a) Isothermal dM/dH vs H curves at different temperatures for $T < T_{N1}$. The inset displays isothermal $M(H)$ data at 2 K, featuring two critical fields (H_{C1} and H_{C2}). (b) The H - T phase diagram for $\text{Fe}_2(\text{MoO}_4)_3$. Data points are derived from metamagnetic transitions (H_{C1} and H_{C2}), and metadielectric transitions ($H_{\epsilon'c1}$ and $H_{\epsilon'c2}$) as shown in (a) and Fig. 3(a). Additionally, $T_{N1}(\chi)$, $T_{N2}(C_p)$, $T_{N2}(\chi)$, $T_{N2}(\epsilon')$, and $T_{N2}(P)$ data points are extracted from Ref. [27]. In (b), white represents the paramagnetic (PM) state, yellow indicates the L -FIM regime, light blue denotes the multiferroic regime, and dark blue represents an unknown phase.

H at different temperatures is presented in Fig. 1(a). The H_{C1} and H_{C2} systematically shift to higher magnetic fields with an increase in temperature, and eventually, H_{C2} disappears for $T \geq 5$ K, while H_{C1} persists close to $T \sim 10$ K. The variation of H_{C1} and H_{C2} with T contrasts with established polar and nonpolar multiferroic systems, where the metamagnetic transition remains rigid with respect to T [37,38]. With the help of new magnetic phase transitions (H_{C1} and H_{C2}), the H - T phase diagram has been reconstructed. The data points in the phase boundaries for $\chi(T, H)$, $C_p(T, H)$, $\epsilon'(T, H)$, and $P(T, H)$ have been taken from Ref. [27]. Further, for completeness, the two metadielectric transitions of $H_{\epsilon'c1}$ and $H_{\epsilon'c2}$ (discussed in Sec. B) data points have also been incorporated in the H - T phase diagram as shown in Fig. 1(b). As seen in the figure, the H_{C1} trend closely resembles the phase boundary between the L -FIM and multiferroic region and both can be inferred to have the same origin. However, a new phase boundary related to H_{C2} below $T < 6$ K, might be related to further modification of the proposed conical spin structure. It is important to mention that the new phase boundary (H_{C2}) does not lead to further changes in the existing polarization, despite the clear change in field-dependent dielectric constant at H_{C2} that indicates it probably arises from the higher-order magnetoelectric coupling. Furthermore, the origins of these H_{C1} and H_{C2} transitions remain unclear and further experimental studies are required to verify the magnetic structure.

To further understand the magnetic behavior, the T -dependent coercive field (H_{co}) and remanent magnetization (M_r) obtained from the isothermal $M(H)$ curves are shown in Fig. 2(a). Here, M_r has a maximum value near T_{N1} and supports the expected L -FIM behavior in $\text{Fe}_2(\text{MoO}_4)_3$ [26]. A similar trend in spontaneous magnetization M_S vs T [inset (ii) of Fig. S4 in the Supplemental Material [33]] further suggests the L -FIM. On the other hand, H_{co} increases with decreasing temperature and displays a peak near $T \sim 5$ K, and then decreases. In general, this behavior is in contrast with the evolution of the FIM nature.

To expose the nature of magnetism in the low- T region, the ac magnetic susceptibility measurements were performed on $\text{Fe}_2(\text{MoO}_4)_3$. Both real (χ') and imaginary (χ'') components of ac susceptibility data, measured at a frequency of 11 Hz with an applied ac magnetic field of 1 Oe, is shown in Fig. 2(b). Here, a sharp peak at $T_{N1} \sim 12$ K is consistent with the $\chi(T)$ data. With a further decrease in T , another magnetic anomaly with a broad hump in χ' and a clear transition in χ'' are observed at $T \sim 6$ K, probably indicating a magnetic glassy phase. Such a low-temperature magnetic anomaly at $T < T_{N1}$ has not been previously reported in the $\text{Fe}_2(\text{MoO}_4)_3$ system. To clarify the spin dynamics of such a low- T magnetic transition, we plotted χ_{phase} against T for various frequencies, as shown in Fig. 2(c). Here, the frequency-independent transition at T_{N1} and frequency-dependent peak below

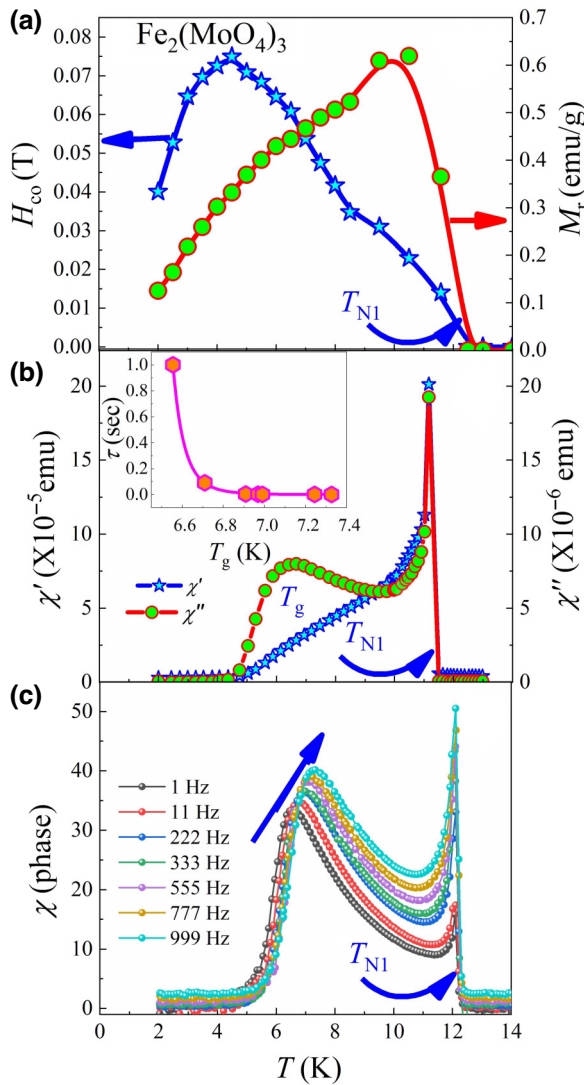


FIG. 2. (a) T -dependent coercive field (H_{co}) (left panel) and remanent magnetization (M_r) (right panel) derived from the isothermal $M(H)$ data. (b) T -dependent in-phase (χ') (left panel) and out-of-phase (χ'') (right panel) components of ac susceptibility for a frequency of 11 Hz. (c) T -dependent χ_{phase} at different frequencies. The inset of Fig. 2(b) shows the fit of the spin-glass temperature (T_g) to the power law (solid line) of Eq. (1).

$T < 7$ K are detailed for different frequencies, and such a frequency-dependent ac susceptibility at low temperatures is clear evidence of magnetic glassy behavior. The frequency-sensitive factor $K = \Delta T_g/[T_{g0}(\log(2\pi f))]$ of spin dynamics, estimated from the χ_{phase} data, is 0.028. According to the different magnetic glass systems classified by Mydosh [39] and in Ref. [40] the obtained “ K ” value is comparable to those of spin-glass systems. Additionally, the change in T_g with relaxation time ($\tau = 1/f$) from χ_{phase} was analyzed with a critical slowing down

model i.e., power law,

$$\tau = \tau_0 \left(\frac{T_g - T_{g0}}{T_g} \right)^{-ZV}, \quad (1)$$

where T_{g0} is the glassy freezing temperature of magnetic glass (as $f \rightarrow 0$ Hz and $H_{\text{dc}} \rightarrow 0$ Oe) and ZV is the critical exponent. A dynamic scaling analysis of χ_{phase} yields the fitting parameters shown in the inset of Fig. 2(b). The microscopic spin relaxation time (τ_0) of 5.7×10^{-9} s, critical exponent $ZV \sim 6.6$, and $T_{g0} \sim 6.2$ K, indicate that the magnetic nature of $\text{Fe}_2(\text{MoO}_4)_3$ below T_g resembles reentry into the spin-glass nature [41–44]. As mentioned previously, the ac magnetic susceptibility study has provided comprehensive insights and confirmed the existence of a hidden low-temperature magnetic phase with reentrant-spin-glass (RSG)-like characteristics in $\text{Fe}_2(\text{MoO}_4)_3$. RSG characteristics have been reported for various magnetic systems, where the dynamics of magnetic glass in long-range magnetically ordered zones are driven by competing magnetic phases resulting from antisite disorder or magnetic inhomogeneities [43]. However, the observed RSG-like nature in $\text{Fe}_2(\text{MoO}_4)_3$ might differ from conventional RSG. In fact, in conventional RSG, the H_{co} sharply increases at the T_g [44].

The possible RSG-like behavior might originate from the thermal evolution of two sublattice magnetizations. In the L -type FIM state, in the ordered magnetic phase, slight differences in exchange interactions lead to distinct rates of thermal evolution for the two sublattice magnetizations [30]. The trends of hyperfine fields for both sublattice magnetizations approaching each other as the temperature approaches zero indicate that antiferromagnetic (AFM) correlation grows at the expense of weak FIM moments. The observed trends suggest that the reentrant-glass-like magnetic phase at T_g may arise from the competition between AFM and FIM domains below T_{N1} . In fact, the peak in the H_{co} vs T curve indicates the growth of AFM domains at low temperatures. This contrasts with conventional RSG behavior, where H_{co} typically exhibits a sharp enhancement below T_g . However, a more detailed analysis is needed to confirm the origin of glassy magnetism in $\text{Fe}_2(\text{MoO}_4)_3$, which is beyond the scope of the present study.

B. Nonlinear magnetodielectric effect and magnetoelectric coupling

$\text{Fe}_2(\text{MoO}_4)_3$ is a magnetically induced multiferroic system below T_{N2} [27]. To understand the correlation between its metamagnetism and dielectric properties, and thus its ME response, we measured the H dependence of magnetodielectric [MD (%)] ($= ((\epsilon'(H) - \epsilon'(0))/\epsilon'(0)) \times 100$) effects at 2 K. Furthermore, to accurately compare dM/dH at 2 K, which is plotted in Fig. 3(a), the H dependence of MD (%) at 2 K is shown in Fig. 3(b). Here, the

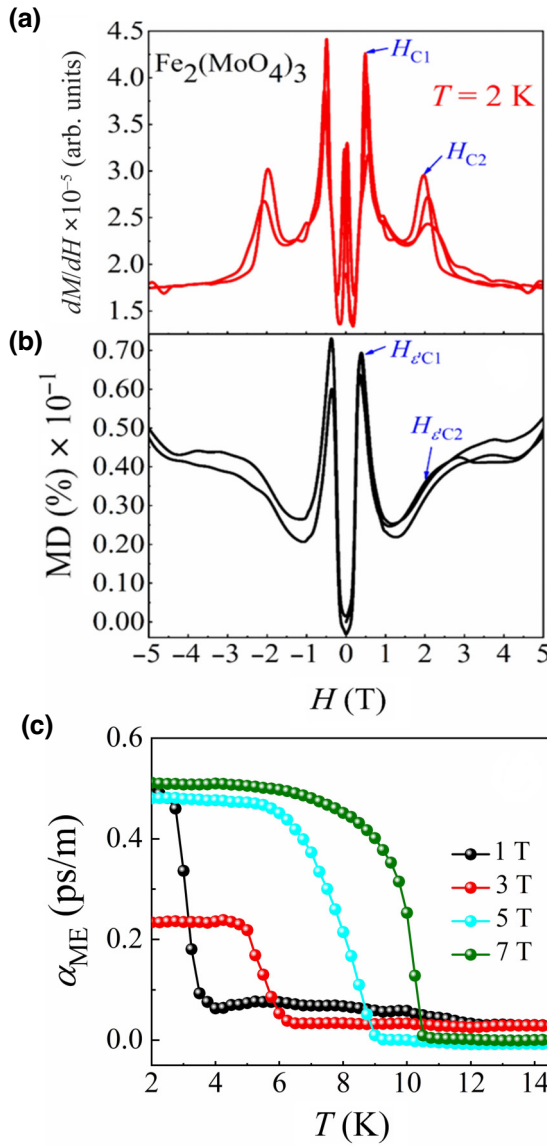


FIG. 3. Isothermal (a) dM/dH vs H curve and (b) MD (%) vs H curve at 2 K. The inflection points H_{C1} and H_{C2} in the dM/dH vs H curve represent the two corresponding metamagnetic transitions. The metadielectric transitions are denoted as $H_{\varepsilon' C1}$ and $H_{\varepsilon' C2}$, respectively. (c) T -dependent magnetoelectric coefficient (α_{ME}) for different H values.

shape of the MD (%) curve changed and remained positive throughout the H range. The presence of such a sharp anomaly in the MD (%) behavior may indicate electrical polarization induced by the magnetic spin structure. The MD (%) varied nonlinearly with H and showed two anomalies, i.e., at $H_{\varepsilon' C1} = 0.51$ T and $H_{\varepsilon' C2} = 1.98$ T, which fitted well to the metamagnetic transition corresponding to two critical magnetic fields H_{C1} and H_{C2} , respectively. Beyond H_{C1} , the MD (%) curve decreased more rapidly, i.e., the lattice polarizability eventually changed; this is likely due to spin reorientation with H , which accounts for the inferred spin structure (possibly

cycloidal order from L -type FIM order). The observation of such one-to-one correspondence between H -induced dM/dH and MD (%) behavior in the same critical magnetic field confirms the strong interaction between magnetic and dielectric coupling. The second metamagnetic transition (at H_{C2}) may contribute to the alteration of magnetic ordering from the speculated cycloidal spin structure to another unknown magnetic ordering. However, a systematic study of isothermal neutron scattering as a function of H is required to unveil the magnetic spin structure, which may be helpful for clarifying the observed nonlinear MD (%) effect in $\text{Fe}_2(\text{MoO}_4)_3$.

As the spin structure altered by H is the anticipated origin of ferroelectric phenomena in $\text{Fe}_2(\text{MoO}_4)_3$, the ME coefficient is estimated by plotting the T -dependent dielectric permittivity (ε') and electric polarization (P) for various H values, as illustrated in Figs. S6(a) and S6(b) in the Supplemental Material [33], respectively. Compared with an individual ferroic material that responds to its

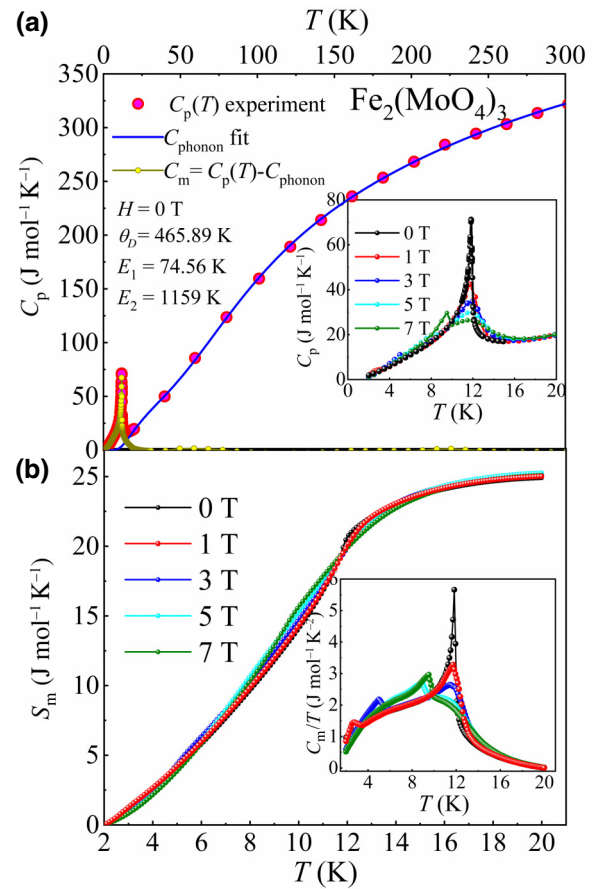


FIG. 4. (a) The T -dependent heat capacity (C_p) under 0 T and the solid line in the main panel are derived from the fitted lattice term (C_{phonon}) described in the text and magnetic specific heat C_m (obtained by subtracting C_{phonon} from C_p). Inset to (a) is the T -dependent C_p in the vicinity of magnetic transition for various H values. (b) The T -dependent magnetic entropy (S_m) and C_m/T [inset to (b)] for different H .

TABLE I. List of systems with multiple caloric effects in composite multiferroic systems and single-phase caloric systems. Here, S. no., S_E , T_E , and T_C denote the serial number, isothermal entropy change due to electric component, electrical induced adiabatic temperature change and magnetic transition temperature respectively.

S. no.	Composite multiferroic	$\Delta S_m/\Delta S_E$ (J kg ⁻¹ K ⁻¹)	ΔT_m (K)	ΔT_E (K)	T_C (K)	Ref.
Composite systems						
1	Pb(Fe _{0.5} Nb _{0.5})O ₃ -BiFeO ₃		0.0015 (5 T)	0.5 (90 kV/cm)	300	[7]
2	La _{0.7} Ca _{0.3} MnO ₃ -BaTiO ₃	-0.7			225	[8]
3	Gd ₅ (Si, Ge) ₄ -PVDF	3			300	[9]
4	BiFeO ₃ - Bi ₄ Ti ₃ O ₁₂			-5.7 (305 kV/cm)	363	[10]
5	Pb(Mn _{1/3} Nb _{2/3})O ₃ -32PbTiO ₃			0.62 K (28 MPa)	323	[11]
6	Eu ₈ Ga ₁₆ Ge ₃₀ -EuO	13			70	[12]
Single-phase caloric systems						
1	BiCu ₃ Cr ₄ O ₁₂	28.2	3.9 (5 T)	5.4 (4.9 kbar)	189	[49]
2	Ni ₅₀ Mn ₃₅ In ₁₅	22.9		-19.7 K (350 MPa)	320	[4]
3	EuTiO ₃			3.66 K (100 kV/cm)	~200	[50]
4	FeRh		20 (7.5 T)	5.31 K (200 MPa)	333	[51]
5	Gd ₅ Ge ₂ Si ₂	13		5.17 (529 MPa)	274	[52]
6	BaTiO ₃	-28			274	[5]
7	FeCr ₂ S ₄	-12		-1.2 (200 MPa)	305	[6]
8	CoCr ₂ S ₄	3.72 (6 K and 5 T) 1.24 (100 kV/m)		0.9 (12 kV/cm and 200 MPa)	6	[53]
		3.99 (28 K and 5 T) 0.56 (100 kV/m)			28	[54]

inherent stimulus, the modulation of P through the application of an external H shows cross coupling between different ferroic states. In the Fe₂(MoO₄)₃ system, the modulation of the L -type FIM to a conical-like spin structure with an external H is directly related to the electric dipoles and contributes to the ME effect. The ME coupling coefficient is estimated by $\alpha_{ME} = (\partial P / \partial H)_E$ and its T -dependence with different H values is plotted as shown in Fig. 3(c). As T decreased, ME coupling began at T_{N2} (which depends on H), increased, and then saturated at low temperatures. Here, α_{ME} was initially large under $H = 1$ T and then began to decrease under 3 T; subsequently, it increased with H . Therefore, α_{ME} exhibited nonlinear behavior for $T < T_{N2}$ and matched well with the variation in spin-spin correlations, as observed in the dM/dH vs H [Fig. 3(a)] and the MD (%) vs H [Fig. 3(b)] plots. The estimated ME effect (α_{ME}) for 7 T at 10 K was approximately 0.56 ps/m, which is comparable to that of known ME materials, such as NdCrTiO₅ [20] and MnGa₂O₄ [45].

C. Field-dependent specific heat capacity and magnetic entropy analysis

Figure 4(a) shows the temperature dependence of specific heat capacity (C_p). For zero field, C_p exhibited an anomaly at around 12 K, which is related to T_{N1} . Furthermore, the concurrent emergence of T_{N2} , caused by the

field-induced spin reorientation (shown in Figs. S3 and S6 in the Supplemental Material [33]) is consistent with the results for $\chi(T, H)$ and $\varepsilon'(T, H)$. The heat capacity (Debye) induced by lattice vibrations was determined by constructing a zero-field $C_p(T)$ curve in the large T region and the data was modeled using one Debye and two Einstein components as shown in Fig. 4(a). Therefore, the Debye-Einstein theory used to describe the lattice-contributed heat capacity C_{phonon} of this system can be expressed as follows [46]:

$$C_{\text{phonon}} = (1 - p - q)9nR \left(\frac{T}{\theta_D} \right)^3 \int_0^{\theta_D/T} \frac{x^4 e^x}{(e^x - 1)^2} dx + 3nR \left[p \frac{(E_1/x)^2 \exp(E_1/x)}{(\exp(E_1/x) - 1)^2} + q \frac{(E_2/x)^2 \exp(E_2/x)}{(\exp(E_2/x) - 1)^2} \right], \quad (2)$$

where n is the number of atoms per molecule [for Fe₂(MoO₄)₃, $n = 17$], R is the universal gas constant, $(1 - p - q)$ is the fraction of vibrational modes contributing to the Einstein-type heat capacity, θ_D is the Debye temperature, and E_1 and E_2 are the Einstein temperatures. The parameters derived by fitting the $C_p(T)$ data to Eq. (2) above 20 K are shown in Fig. 4(a). The extracted lattice-contributed heat capacity (C_{phonon}) was subtracted from

the total $C_p(T)$ data to determine the spin-contributed heat capacity (C_m).

In addition to the magnetic entropy associated with the FIM order at 12 K, $(C_m/T)dT$ was integrated, and the corresponding spin entropy (S_m) is shown in Fig. 4(b). For a zero magnetic field, the calculated saturation value of $S_m \sim 25 \text{ J mol}^{-1} \text{ K}^{-1}$, which is the maximum entropy theoretically estimated from the spin-only contribution of Fe^{3+} ($S = 5/2$), $29.8 \text{ J mol}^{-1} \text{ K}^{-1}$ [$S_m = 2R\ln(2S+1)$]. This suggests that more than 84% of the spin entropy is emitted just below the FIM order and that slight difference in S_m is due to Fe^{3+} ions not having full effective spin at low T values [47,48].

D. Solid-state refrigeration phenomena: Magnetic-field-induced total adiabatic temperature change

The coexistence of multiple order parameters and the associated entropy changes during phase transitions facilitate investigations into multicaloric phenomena in multiferroic systems. Table I summarizes the reported multiple caloric effects resulting from individual caloric behaviors in composite and single-phase multiferroics [4–12,49–54]. As $\text{Fe}_2(\text{MoO}_4)_3$ is a field-induced multiferroic system with a phase transition from the *L*-type FIM state to the proposed conical spin structure and exhibits significant changes in magnetic susceptibility, it may display a large multicaloric effect owing to its intricate ME coupling. Using Maxwell's equations, the MCE with isothermal entropy change ($-\Delta S_m$) is estimated for different H ranging from 1 to 7 T at specified T values, as shown in the Fig. S7(a) Supplemental Material [33]. At $H = 1$ T, $-\Delta S_m$ showed a peak around T_{N1} , and it increased at lower T , which agrees well with the magnetic-field-induced T_{N2} . This feature became more evident as H increased; eventually, $-\Delta S_m$ exhibited oscillatory-like behavior due to the conventional magnetocaloric effect and the inverse (or negative) magnetocaloric effect (IMCE) over the entire temperature range [55]. As expected, the IMCE peak became stronger as H increased and shifted systematically to higher T , as indicated by the measurements of $\chi(T, H)$ and $\varepsilon'(T, H)$ shown in Figs. S3(c), S3(d), and S6 in the Supplemental Material [33]. Such an oscillating MCE (i.e., $-\Delta S_m$) as a function of T and H can be attributed to the T_{N2} induced by H . Additionally, $-\Delta S_m$ was calculated from the field-dependent heat-capacity data, as shown in Fig. S7(b) in the Supplemental Material [33], using the relation,

$$\Delta S_m = \int_0^T \frac{C_m(H_2, T) - C_m(H_1, T)}{T} dT. \quad (3)$$

The calculated MCE and its qualitative behavior agreed well with the results obtained from the isothermal $M(H)$.

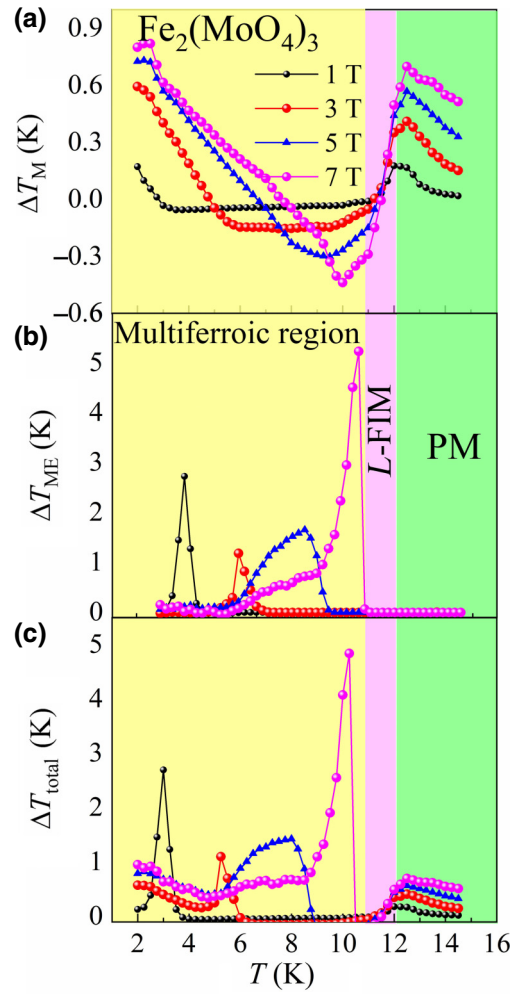


FIG. 5. (a) Magnetically induced adiabatic temperature change ΔT_m vs T , (b) adiabatic temperature change due to magnetoelectric coupling ΔT_{ME} vs T , and (c) the total adiabatic temperature change ΔT_{total} vs T for different H values in various temperature regimes (green, PM state; pink, *L*-FIM regime; and yellow, multiferroic regime).

Meanwhile, the magnetically induced adiabatic temperature change (ΔT_m) was estimated from the isoentropic difference between $S(0, T)$ and $S(H, T)$ as follows:

$$\Delta T_m = \frac{-T}{C_p} \Delta S_m. \quad (4)$$

The results are shown in Fig. 5(a). The observed ΔT_m was positive with a maximum value of 0.81 K below T_{N2} , whereas it was negative for $T_{N2} < T < T_{N1}$, with a magnitude of -0.43 K at T_{N2} . Finally, there was a positive MCE with a maximum $\Delta T_m \sim 0.7$ K near T_{N1} .

Recently, Vopson [13,14] reported that coupled systems with multiple ferroic properties are suitable for expressing significant adiabatic temperature changes ($\Delta T_{\text{total}} = \Delta T_m + \Delta T_{ME}$) [56]. As discussed previously, in addition to the good ME coupling of $\text{Fe}_2(\text{MoO}_4)_3$, its

TABLE II. Magnetoelectric coupling-induced multicaloric effect in single-phase multiferroic compounds. Here, S. no. and T_N denotes the serial number and magnetic transition respectively.

S. no.	Multiferroic	Transition temperature T_C (K)	ME coupling constant α_{ME} (ps/m)	ΔT_m (K) at 7 T	ΔT_{ME} (K) at 7 T	ΔT_{total} (K) at 7 T	Ref.
1	$Fe_2(MoO_4)_3$	12	0.56 at $T = 2$ K	0.7 at T_{N1} −0.43 at T_{N2} 0.8 at 2 K	5.2 at T_{N2}	4.8 at T_{N2} and 0.7 at T_{N1}	This work
2	Y_2CoMnO_6	75	0.41 at $T = 75$ K	5.45 at 75 K	0.34 at 75 K	5.79 at T_N	[21]
3	$NdCrTiO_5$	21	0.5 at $T = 21$ K	6.3 at 21 K	0.58 at $T = 21$ K	6.88 at T_N	[20]

low magnetic hysteresis and low specific heat capacity (approximately 0.2 mJ K^{−1} at 10 K) render it susceptible to a strong adiabatic cooling response. Theoretically, multiferroic SrMnO₃ is predicted to contribute 60% of its entropy change through its significant ME coupling [57]. Therefore, considering ME coupling, the total adiabatic temperature change (ΔT_{total}) of $Fe_2(MoO_4)_3$ was estimated based on using H under the effects of electrical quantities such as polarization and dielectric response [58]. A change in the magnetic structure induces electric polarization, thus resulting in an internal electric field (E) with an ME effect of $dE_{in} = (\alpha_{ME}/\epsilon_0\chi^e)dH$, where α_{ME} is the ME coupling coefficient, ϵ_0 the permittivity of free space, and χ^e ($=\epsilon' - 1$, where ϵ' is the relative dielectric constant) the electrical susceptibility. Thus, the ΔT_{total} of $Fe_2(MoO_4)_3$ under the effect of H , as derived from the generalized Maxwell relation, is as follows:

$$\Delta T_{total} = \frac{-T}{C_P} \int_{H_i}^{H_f} \left[\left(\frac{\partial M}{\partial T} \right)_{H,E} + \frac{\alpha_{ME}}{\chi^e \epsilon_0} \left(\frac{\partial P}{\partial T} \right)_{H,E} \right] dH. \quad (5)$$

Here, the first term represents the individual adiabatic temperature change due to the MCE (ΔT_m), and the second term represents the adiabatic temperature change (ΔT_{ME}) due to the ME coupling. Using the available data, the combined effect of adiabatic temperature changes due to the ME effect (ΔT_{ME}) and ΔT_{total} was estimated and plotted as a function of T for different H values, as shown in Figs. 5(b) and 5(c), respectively. Here, the estimation yielded two peaks in ΔT_{total} for all H . One peak was due to a single MCE of magnitude 0.7 K near T_{N1} , and the other peak exhibited a large magnitude of approximately 5.2 K at T_{N2} owing to the isothermal temperature change caused by ME coupling. As shown in Figs. 5(a)–5(c), the contribution of the standard MCE to the total adiabatic temperature change was insignificant, i.e., −0.43 K. However, the contribution from ME coupling to ΔT_{total} was significant, with a magnitude of 5.2 K at T_{N2} for $H = 7$ T. This combined caloric effect resulted in a cooling temperature of approximately 4.8 K for T_{N2} . The ΔT_{total} induced by ME coupling was comparable to that of other magnetically induced multiferroic systems (see Table II [20,21]).

$Fe_2(MoO_4)_3$ offers an important advantage in that, for all single-phase and composite multiferroic or nonmultiferroic systems, it allows the maximum observed adiabatic temperature change to be adjusted via an external H whose temperature is similar to the ordering temperature. However, in the $Fe_2(MoO_4)_3$ system, the temperature regime corresponds to a significant adiabatic temperature change, and because T_{N2} is a function of H , the cooling efficiency varies with the external H . This peculiar field-dependent tuning behavior of the temperature zone for the large caloric effect is specific to the $Fe_2(MoO_4)_3$ multiferroic system.

IV. CONCLUSIONS

This study provides insights into the *L*-type FIM behavior of $Fe_2(MoO_4)_3$ and highlights some important findings. The detailed H - T phase diagram obtained from isothermal magnetization studies revealed an additional phase boundary (H_{C2}) extending beyond the known multiferroic boundary (H_{C1}). Furthermore, the evident dielectric anomalies coupled with the nonlinear MD behavior associated with H_{C1} and H_{C2} highlighted the complex interplay between the electric and magnetic orders. The frequency-dependent ac susceptibility revealed concealed RSG-like behavior at $T_{g0} = 6.2$ K, which is below T_{N1} . Additionally, numerical calculations to estimate the MCE ($\Delta T_m = 0.8$ K) arising from magnetic contributions indicated low values and oscillating behavior. ME coupling induced a significant adiabatic temperature change near T_{N2} ($\Delta T_{ME} = 5.2$ K at 7 T), and demonstrated flexibility in temperature and magnetic field parameters. Therefore, the observed solid-state cooling effects with respect to temperature and magnetic field variations suggest that the multiferroic system $Fe_2(MoO_4)_3$ is promising for practical applications in future cooling devices, particularly in low-temperature solid-state caloric applications.

ACKNOWLEDGMENTS

P.A. thanks NIT Andhra Pradesh for financial support and J.K. thanks DST-GITA, India under Grant No. GITA/DST/TWN/P-90/2021. This study was supported by

the National Science and Technology Council, Taiwan, under Grants No. MOST 110-2112-M-110-008-MY3, No. NSTC 111-2112-M-110-019, No. NSTC 111-2811-M-110-010, No. NSTC 112-2811-M-110-029, No. NSTC 112-2923-M-110-001, and No. NSTC 112-2112-M-110-018.

-
- [1] K. Yoo, B. Koteswararao, J. Kang, A. Shahee, W. Nam, F. F. Balakirev, V. S. Zapf, N. Harrison, A. Guda, N. Ter-organessian, and K. H. Kim, Magnetic field-induced ferroelectricity in $S = 1/2$ kagome staircase compound $\text{PbCu}_3\text{TeO}_7$, *npj Quantum Mater.* **3**, 45 (2018).
- [2] N. D. Khanh, N. Abe, H. Sagayama, A. Nakao, T. Hanashima, R. Kiyanagi, Y. Tokunaga, and T. Arima, Magnetoelectric coupling in the honeycomb antiferromagnet $\text{Co}_4\text{Nb}_2\text{O}_9$, *Phys. Rev. B* **93**, 075117 (2016).
- [3] A. Maignan and C. Martin, $\text{Fe}_4\text{Nb}_2\text{O}_9$: A magnetoelectric antiferromagnet, *Phys. Rev. B* **97**, 161106(R) (2018).
- [4] Z. Li, Z. Li, D. Li, J. Yang, B. Yang, Y. Hu, D. Wang, Y. Zhang, C. Esling, X. Zhao, and L. Zuo, Achieving a broad refrigeration temperature region through the combination of successive caloric effects in a multiferroic $\text{Ni}_{50}\text{Mn}_{35}\text{In}_{15}$ alloy, *Acta Mater.* **192**, 52 (2020).
- [5] A. Magnus, G. Carvalho, C. S. Alves, A. De Campos, A. A. Coelho, S. Gama, F. C. G. Gandra, P. J. Von Ranke, and N. A. Oliveira, The magnetic and magnetocaloric properties of $\text{Gd}_5\text{Ge}_2\text{Si}_2$ compound under hydrostatic pressure, *J. Appl. Phys.* **97**, 10M320 (2005).
- [6] S. Yuce, M. Barrio, B. Emre, E. Stern-Taulats, A. Planes, J. L. Tamarit, Y. Mudryk, K. A. Gschneidner, V. K. Pecharsky, and L. Mañosa, Barocaloric effect in the magnetocaloric prototype $\text{Gd}_5\text{Si}_2\text{Ge}_2$, *Appl. Phys. Lett.* **101**, 071906 (2012).
- [7] U. Prah, M. Wencka, T. Rojac, A. Benčan, and H. Uršič, $\text{Pb}(\text{Fe}_{0.5}\text{Nb}_{0.5})\text{O}_3$ - BiFeO_3 -based multicalorics with room-temperature ferroic anomalies, *J. Mater. Chem. C* **8**, 11282 (2020).
- [8] X. Moya, L. E. Hueso, F. Maccherozzi, A. I. Tovstolytkin, D. I. Podyalovskii, C. Ducati, L. C. Phillips, M. Ghidini, O. Hovorka, A. Berger, M. E. Vickers, E. Defay, S. S. Dhesi, and N. D. Mathur, Giant and reversible extrinsic magnetocaloric effects in $\text{La}_{0.7}\text{Ca}_{0.3}\text{MnO}_3$ films due to strain, *Nat. Mater.* **12**, 52 (2013).
- [9] V. M. Andrade, A. Amirov, D. Yusupov, B. Pimentel, N. Barroca, A. L. Pires, J. H. Belo, A. M. Pereira, M. A. Valente, J. P. Araújo, and M. S. Reis, Multicaloric effect in a multiferroic composite of $\text{Gd}_5(\text{Si}, \text{Ge})_4$ microparticles embedded into a ferroelectric PVDF matrix, *Sci. Rep.* **9**, 18308 (2019).
- [10] Z. Tang, Y. Zhou, B. Yang, J. Chen, and S. Zhao, Giant negative electrocaloric effect over a wide temperature region (263–373 K) in lead-free $\text{BiFeO}_3/\text{B}_4\text{Ti}_3\text{O}_{12}$ composite films, *J. Phys. Chem. Solids* **172**, 111054 (2023).
- [11] A. Chauhan, S. Patel, and R. Vaish, Multicaloric effect in $\text{Pb}(\text{Mn}_{1/3}\text{Nb}_{2/3})\text{O}_3$ - 32PbTiO_3 single crystals, *Acta Mater.* **89**, 384 (2015).
- [12] A. Chaturvedi, S. Stefanoski, M. H. Phan, G. S. Nolas, and H. Srikanth, Table-like magnetocaloric effect and enhanced refrigerant capacity in $\text{Eu}_8\text{Ga}_{16}\text{Ge}_{30}$ - EuO composite materials, *Appl. Phys. Lett.* **99**, 162513 (2011).
- [13] M. M. Vopson, Theory of giant-caloric effects in multiferroic materials, *J. Phys. D: Appl. Phys.* **46**, 345304 (2013).
- [14] M. M. Vopson, The multicaloric effect in multiferroic materials, *Solid State Commun.* **152**, 2067 (2012).
- [15] A. Tiwari, D. Chandrasekhar Kakarla, B. Poojitha, P. Sahoo, H. L. Liu, A. Dixit, C. W. Wang, T. W. Yen, M. J. Hsieh, J. Y. Lin, J. Krishnamurthy, Y. C. Lai, H. Chou, T. W. Kuo, A. Pal, and H. D. Yang, Spin-phonon-charge coupling in the two-dimensional honeycomb lattice compound $\text{Ni}_2\text{Te}_3\text{O}_8$, *Phys. Rev. B* **108**, 075113 (2023).
- [16] A. Pal, T. W. Yen, T. W. Kuo, C. W. Wang, S. M. Huang, M. C. Chou, Y. C. Lai, Y. C. Chuang, P. Yanda, A. Sundaresan, H. S. Kunwar, V. G. Sathe, Ajay Tiwari, D. Chandrasekhar Kakarla, and H. D. Yang, Unconventional multiferroicity induced by structural distortion and magnetostriction effect in the layered spin-1/2 ferrimagnet $\text{Bi}_2\text{Cu}_5\text{B}_4\text{O}_{14}$, *Phys. Rev. B* **107**, 184430 (2023).
- [17] C. H. Prashanth, T. W. Yen, Ajay Tiwari, P. Athira, S. M. Huang, B. Poojitha, D. P. Gulo, H. L. Liu, C. W. Wang, Y. K. Lin, Y. C. Lai, J. Krishnamurthy, H. D. Yang, and D. Chandrasekhar Kakarla, Interplay of magnetic and electric coupling across the spin density wave to conical magnetic ordering in a BaHoFeO_4 spin-cluster chain compound, *J. Alloys Compd.* **942**, 169017 (2023).
- [18] D. Chandrasekhar Kakarla, H. C. Wu, D. J. Hsieh, P. J. Sun, G. J. Dai, J.-Y. Lin, J. L. Her, Yasuhiro H. Matsuda, L. Z. Deng, M. Gooch, C. W. Chu, and H. D. Yang, Metamagnetic transitions and magnetoelectric coupling in acentric and nonpolar Pb_2MnO_4 , *Phys. Rev. B* **99**, 195129 (2019).
- [19] S. Lisenkov, B. K. Mani, C. M. Chang, J. Almand, and I. Ponomareva, Multicaloric effect in ferroelectric PbTiO_3 from first principles, *Phys. Rev. B* **87**, 224101 (2013).
- [20] J. Hwang, E. S. Choi, H. D. Zhou, J. Lu, and P. Schlottmann, Magnetoelectric effect in NdCrTiO_5 , *Phys. Rev. B* **85**, 024415 (2012).
- [21] J. Krishnamurthy and A. Venimadhav, Multicaloric effect in multiferroic Y_2CoMnO_6 , *J. Phys. D: Appl. Phys.* **47**, 445002 (2014).
- [22] L. E. Cross, A. Fouksova, and S. E. Cummins, Gadolinium molybdate, a new type of ferroelectric crystal, *Phys. Rev. Lett.* **21**, 812 (1968).
- [23] J. D. Axe, B. Dorner, and G. Shirane, Mechanism of the ferroelectric phase transformation in rare-earth molybdates, *Phys. Rev. Lett.* **26**, 519 (1971).
- [24] A. W. Sleight and L. H. Brixner, A new ferroelastic transition in some $\text{A}_2(\text{MO}_4)_3$ molybdates and tungstates, *J. Solid State Chem.* **7**, 172 (1973).
- [25] D. Chandrasekhar Kakarla, J. Krishnamurthy, J.-Y. Lin, H. C. Wu, and H. D. Yang, Observation of oscillation like magnetocaloric effect in multiferroic $\text{Ni}_{0.95}\text{Zn}_{0.05}\text{Cr}_2\text{O}_4$, *J. Alloys Compd.* **771**, 674 (2019).
- [26] G. J. Long, *Chemical Mössbauer Spectroscopy* (Springer, Boston, MA, 1984).
- [27] A. Tiwari, D. Chandrasekhar Kakarla, M. J. Hsieh, J. Y. Lin, C. W. Wang, L. K. Tseng, C. E. Lu, A. Pal, T. W. Kuo, M. M. C. Chou, and H. D. Yang, Observation of magnetic field-induced second magnetic ordering and peculiar

- ferroelectric polarization in L-type ferrimagnetic $\text{Fe}_2(\text{MoO}_4)_3$, *Phys. Rev. Mater.* **6**, 094412 (2022).
- [28] P. D. Battle, A. K. Cheetham, N. J. Pollard, W. T. A. Harrison, C. C. Laboratories, P. Road, and T. Division, The structure and magnetic properties of chromium(III) molybdate, *J. Solid State Chem.* **58**, 221 (1985).
- [29] H. Chen, The crystal structure and twinning behavior of ferric molybdate, $\text{Fe}_2(\text{MoO}_4)_3$, *Mater. Res. Bull.* **14**, 1583 (1979).
- [30] P. D. Battle, A. K. Cheetham, G. J. Long, and G. Longworth, Study of the magnetic properties of iron (III) molybdate, by susceptibility, Mössbauer, and neutron diffraction techniques, *Inorg. Chem.* **21**, 4223 (1982).
- [31] H. Ehrenberg, K. G. Bramnik, E. Muessig, T. Buhrmester, H. Weitzel, and C. Ritter, The ferrimagnetic structure of $\text{Fe}_2\text{Mo}_3\text{O}_{12}$: dependence of Fe-O-O-Fe superexchange couplings on geometry, *J. Magn. Magn. Mater.* **261**, 353 (2003).
- [32] W. Song, B. Yuan, X. Liu, Z. Li, J. Wang, and E. Liang, Tuning the monoclinic-to-orthorhombic phase transition temperature of $\text{Fe}_2\text{Mo}_3\text{O}_{12}$ by substitutional co-incorporation of Zr^{4+} and Mg^{2+} , *J. Mater. Res.* **29**, 849 (2014).
- [33] See Supplemental Material <http://link.aps.org/supplemental/10.1103/PhysRevApplied.21.054025> for Rietveld refinement of XRD, crystal structure, magnetization, temperature, and field-dependent dielectric permittivity, polarization, and isothermal entropy change data of $\text{Fe}_2(\text{MoO}_4)_3$.
- [34] T. Roisnel and J. Rodriguez-Carvajal, WinPLOTR: A windows tool for powder diffraction pattern analysis, *Mater. Sci. Forum* **378**, 118 (2000).
- [35] K. Momma and F. Izumi, VESTA 3 for three-dimensional visualization of crystal, volumetric and morphology data, *J. Appl. Cryst.* **44**, 1272 (2011).
- [36] Z. Jirak, R. Salmon, L. Fournes, F. Menil, and P. Hagemuller, Magnetic and Mössbauer resonance investigations of the weak ferrimagnetic iron molybdate ($\text{Fe}_2(\text{MoO}_4)_3$), *Inorg. Chem.* **21**, 4218 (1982).
- [37] M. T. Okunaga, M. A. Zuma, and Y. S. Himakawa, High-field study of strong magnetoelectric coupling in single-domain crystals of BiFeO_3 , *J. Phys. Soc. Japan* **79**, 064713 (2010).
- [38] J. Krishnamurthy, D. Chandrasekhar Kakarla, H. C. Wu, H. D. Yang, J. Y. Lin, and A. Venimadhav, Metamagnetic behaviour and effect of field cooling on sharp magnetization jumps in multiferroic Y_2CoMnO_6 , *Euro. Phys. Lett.* **108**, 27013 (2014).
- [39] J. A. Mydosh, *Spin Glasses: An Experimental Introduction* (Taylor & Francis, London, 1993).
- [40] S. Bedanta and W. Kleemann, Supermagnetism, *J. Phys. D: Appl. Phys.* **42**, 013001 (2009).
- [41] M. Viswanathan and P. S. AnilKumar, Observation of reentrant spin glass behavior in $\text{LaCo}_{0.5}\text{Ni}_{0.5}\text{O}_3$, *Phys. Rev. B* **80**, 012410 (2009).
- [42] K. Jonason, J. Mattsson, and P. Nordblad, Dynamic susceptibility of a reentrant ferromagnet, *Phys. Rev. B* **53**, 6507 (1996).
- [43] D. Choudhury, P. Mandal, R. Mathieu, A. Hazarika, S. Rajan, A. Sundaresan, U. V. Waghmare, R. Knut, O. Karis, P. Nordblad, and D. D. Sarma, Near-room-temperature colossal magnetodielectricity and multiglass properties in partially disordered $\text{La}_2\text{NiMnO}_6$, *Phys. Rev. Lett.* **108**, 127201 (2012).
- [44] J. Dho, W. S. Kim, and N. H. Hur, Reentrant spin glass behavior in Cr-doped perovskite manganite, *Phys. Rev. Lett.* **89**, 027202 (2002).
- [45] R. Saha, S. Ghara, E. Suard, D. H. Jang, K. H. Kim, N. V. Ter-Oganessian, and A. Sundaresan, Magnetoelectric effect in simple collinear antiferromagnetic spinel, *Phys. Rev. B* **94**, 014428 (2016).
- [46] R. Kumar and A. Sundaresan, Unveiling a hidden multiferroic state under magnetic fields in BaHoFeO_4 , *Phys. Rev. B* **107**, 184420 (2023).
- [47] P. J. Baker, H. J. Lewtas, S. J. Blundell, T. Lancaster, I. Franke, W. Hayes, F. L. Pratt, L. Bohatý, and P. Becker, Muon-spin relaxation and heat capacity measurements on the magnetoelectric and multiferroic pyroxenes $\text{LiFeSi}_2\text{O}_6$ and $\text{NaFeSi}_2\text{O}_6$, *Phys. Rev. B* **81**, 214403 (2010).
- [48] A. M. Tishin, K. A. Gschneidner, and V. K. Pecharsky, Magnetocaloric effect and heat capacity in the phase-transition region, *Phys. Rev. B* **59**, 503 (1999).
- [49] Y. Kosugi, M. Goto, Z. Tan, D. Kan, and M. Isobe, Giant multiple caloric effects in charge transition ferrimagnet, *Sci. Rep.* **11**, 12682 (2021).
- [50] Y. Q. Zhao and H. X. Cao, Multicaloric effect in multiferroic EuTiO_3 thin films, *J. Mater. Sci.* **55**, 5705 (2020).
- [51] S. A. Nikitin, G. Myalikgulyev, A. M. Tishin, M. P. Annaorazov, K. A. Asatryan, and A. L. Tyurin, The magnetocaloric effect in $\text{Fe}_{49}\text{Rh}_{51}$ compound, *Phys. Lett. A* **148**, 363 (1990).
- [52] S. A. Nikitin, G. Myalikgulyev, M. P. Annaorazov, A. L. Tyurin, R. W. Myndyev, and S. A. Akopyan, Giant elastocaloric effect in FeRh alloy, *Phys. Lett. A* **171**, 234 (1992).
- [53] Y. Liu, J. Wei, P. E. Janolin, I. C. Infante, X. Lou, and B. Dkhil, Giant room-temperature barocaloric effect and pressure-mediated electrocaloric effect in BaTiO_3 single crystals, *Appl. Phys. Lett.* **104**, 162904 (2014).
- [54] K. Dey, A. Indra, A. Karmakar, and S. Giri, Multicaloric effect in multiferroic sulpho spinel MCr_2S_4 ($\text{M} = \text{Fe} \& \text{Co}$), *J. Magn. Magn. Mater.* **498**, 166090 (2020).
- [55] P. Gupta and P. Poddar, Study of magnetic and thermal properties of SmCrO_3 polycrystallites, *RSC Adv.* **6**, 82014 (2016).
- [56] Z. Jiang, B. Xu, S. Prosandeev, Y. Nahas, S. Prokhorenko, J. Íñiguez, and L. Bellaiche, Electrocaloric effects in multiferroics, *Phys. Rev. B* **103**, L100102 (2021).
- [57] A. Edström and C. Ederer, Prediction of a giant magnetoelectric cross-caloric effect around a tetracritical point in multiferroic SrMnO_3 , *Phys. Rev. Lett.* **124**, 167201 (2020).
- [58] A. Kumar and K. L. Yadav, Study on multicaloric effect of CuO induced multiferroic, *J. Appl. Phys.* **116**, 083907 (2014).